Methylene blue-containing liposomes as new photodynamic anti-bacterial agents.

Daniele Bani[¥], Andrea Bencini[†], Debora Berti[‡], Giulia Boccalini[¥], Luca Conti[†,*], Claudia Giorgi[†], Alessio Mengoni[§], Costanza Montis[‡], Barbara Valtancoli[†].

[†] Department of Chemistry Ugo Schiff, University of Florence, Via della Lastruccia 3, 50019, Sesto Fiorentino (FI), Italy.

[¥] Department of Experimental & Clinical Medicine, Research Unit of Histology & Embryology, University of Florence, Italy.

[‡] Department of Chemistry Ugo Schiff and CSGI, University of Florence, Via della Lastruccia 3, 50019, Sesto Fiorentino (FI), Italy.

[§] Department of Biology, University of Florence, via Madonna del Piano 6, 50019, Sesto Fiorentino (FI), Italy.

* Author for correspondence: +0390554573299

E-mail address: luca.conti@unifi.it

ABSTRACT

Methylene blue (MB) is of great interest for biomedical applications. In particular, due to its ability to release oxygen free radicals upon photo-activation, it can be employed as photoactivated anti-microbial drug in photodynamic therapy (PDT). However, the poor ability of the MB itself to penetrate bacterial cell walls and bacterial biofilms determines a strong limitation of its antimicrobial activity. In this paper we propose a strategy to improve the MB antimicrobial efficacy based of different cationic liposomal formulations. Liposomes-MB systems were physico-chemically characterized by Dynamic Light Scattering (DLS), Zeta Potential and UV-visible spectroscopy. Their ability to penetrate inside the cytoplasm of *E. coli*, taken as Gram-negative bacterial model, was investigated through Laser Scanning Confocal Microscopy (CLSM) and compared to the ability of bare MB. The study of antimicrobial activity of the MB-loaded liposomes upon photo-activation on *E. coli* bacteria, demonstrated that liposomes-based formulations improve the effect of MB as antibacterial agent. Furthermore, we were able to establish a clear correlation between the physico-chemical features of liposome formulations and their antimicrobial efficacy, providing fundamental knowledge for the development of novel efficient PDT treatments.

Keywords: Methylene Blue, Drug Delivery, Liposomes, Photodynamic Therapy, Antimicrobial agents, Periodontic Disease.

INTRODUCTION

Nowadays photodynamic therapy (PDT) represents one of the most promising approaches for the treatment of a wide variety of pathologies[1-2-3-4-5-6]. It has found application mainly as an alternative to chemotherapy or radiotherapy of lung, gastric, cervical, colorectal, esophageal, head and neck malignancies[7–9-10,] as well as for non-neoplastic diseases in opthalmology, gastroenterology, cardiology, and neonatology[11]. Of particular relevance, PDT is largely employed in dermatology, for the treatment of inflammatory/degenerative skin disorders, including actinic keratosis, acne vulgaris, psoriasis and aging-related pathologies[12-13]. In general, the principle of PDT is based on systemic or local administration of a non-toxic photosensitizer (PS) drug, able to absorb energy from a light source with appropriate wavelength and power. The PS agent can then activate two distinct mechanisms. It may give rise to electron transfer reactions generating reactive oxygen molecules (ROS), able to induce radical damages (Type I), or, in the presence of oxygen, it can in turn transfer the energy to surrounding oxygen molecules, producing singlet oxygen ($^1O_2$), one of the most potent cytotoxic species (Type II)[14-15]. These processes can cause severe oxidative damage to biological macromolecules, such as DNA of cancer cells or bacteria, thereby inducing cell death and tissue destruction *in vivo*[16]. The main advantage of PDT with respect to conventional treatments lies on the possibility to localize the photo-activation of the PS agent, and thus the cytotoxic effect, into the targeted tissue. This allows to decrease the occurrence and severity of unwanted side effects and to repeat the treatment until achievement of the desired therapeutic effects[17]. Moreover, when combined with surgery and/or chemotherapy, PDT may enhance the treatment efficacy and prevent metastasis. On the other hand, the major limitation of therapies based on a photo-excitable molecule

producing singlet oxygen is represented by the very short lifetime of the latter (< 0.04 μs) in biological systems, determining a scarce tissue penetration (< 0.02 mm), and thus limiting their successful application to small superficial tumors[18].

Recently, due to the rising issue of antibiotic resistance, there has been an increasing interest in developing new PDT-based antibacterial treatments for many infection diseases, like periodontitis[19-20-21]. In fact, the PDT approach would be advantageous with respect to traditional antibiotic therapies, since it allows killing bacteria through the photo-induced generation of ROS, avoiding the appearance of drug-resistant strains[22]. Several PS have been investigated for their ability to bind and inactivate bacteria and, in particular, it is well known that neutral or anionic PS agents are able to efficiently inactivate Gram-positive bacteria while Gram-negative bacteria are relatively resistant to these compounds. This behavior can be attributed to the peptidoglycan and lipoteichoic acid surrounding of the Gram-positive cytoplasmic membrane, that are more easily crossed with respect to the outer cell membrane of Gram-negative bacteria[23]. For this reason, several methods for the PDT treatment of Gram-negative bacteria have been recently proposed, involving the use of polycationic peptides or phenothiazinium dyes like toluidine blue or methylene blue, to afford a better penetration of the PS agent through the outer membrane and thus allowing the photo-induced ROS generation in a more fatal location of the cell[24-25]. However, the efficacy of this technique is reduced by biological barriers (cell wall and cell membrane), which impede access of the drug to the interior of bacteria, where photoactivation can damage the endocellular targets. Moreover, the organization of bacterial colonies in biofilms makes them very poorly accessible to drugs, due to production of extracellular polymers which physically limit the permeability of therapeutics[26,27]. In this respect, the encapsulation of an active PS agent in a proper carrier can be a useful strategy to improve its capacity to reach

effective levels into its biological target and to perform its therapeutic antimicrobial activity. Among the drug delivery systems (DDS), lipid assemblies and liposomes in particular, are the most employed thanks to their high biocompatibility and ability to easily host high amounts of hydrophilic active molecules in their inner aqueous pool[28-29-30-31]. Furthermore, their chemical composition can be appropriately tuned to improve their efficiency as drug carriers, depending on the pathogenic species to be targeted.

In this study we designed, developed and characterized different nano-formulations of MB (Methylene Blue)-loaded liposomes, made of a mixture of a cationic lipid, dimethyldioctadecylammonium chloride (DOTAC), cholesterol (Chol) and dipalmitoylphosphatidylcholine (DPPC). Their composition was varied in order to study the efficacy towards bacteria of formulations featuring different physico-chemical properties, such as superficial charges and mean diameters. These properties were analyzed by means of dynamic light scattering (DLS) and zeta potential measurements, and emerged to have a major influence in the modulation of antibacterial efficacy and capability to penetrate bacterial biofilms. The ability of MB-containing liposomes to interact with bacteria was evaluated using *in vitro* cultures of *E. coli*, a Gram-negative bacterium taken as paradigm of aggressive microbial species, by means of laser scanning confocal microscopy (CLSM). The anti-microbial efficacy of the different liposome formulations upon photoexcitation was tested through CLSM and cell viability assays, with the aim to qualitatively and quantitatively compare the efficiency of MB-liposomes and free MB for PDT purposes, also against bacterial biofilms. Finally, the ability of photoexcited MB-containing liposomes to inactivate lipopolysaccharide (LPS), a major pro-inflammatory endotoxin of Gram- bacteria was investigated, in order to complete a thorough

characterization of the developed systems as PDT drugs, both in terms of bacterial inactivation and of anti-inflammatory therapeutic action.

RESULTS AND DISCUSSION

Preparation and characterization of liposomes. Liposomes were prepared in five different lipid formulations, in order to investigate the interaction and the bactericidal efficacy of structures with different properties. We prepared four MB-containing liposomes (**Lip 1-4**) plus one empty liposome not carrying MB (**Lip E**) prepared as **Lip 1** and employed as a reference negative control: their composition and the structures of the single components of the different formulations, are reported in **Table 1** and **Figure 1**, respectively.

Table 1. Molar ratios of the three components employed for the preparation of liposomes: DODAC (dimethyldioctadecylammonium chloride), DPPC (dipalmitoylphosphatidylcholine), Chol (cholesterol), for the four different formulations loaded with MB (Lip 1, Lip 2, Lip 3, Lip 4), characterized by increasing cationic lipid (DODAC) amount, plus the empty liposome Lip E.

	DPPC/ Chol/ DODAC
Lip 1	1:0.5:0.3
Lip 2	1:0.5:0.5
Lip 3	1:0.5:0.8
Lip 4	1:0.5:1.2
Lip E	1:0.5:0.3

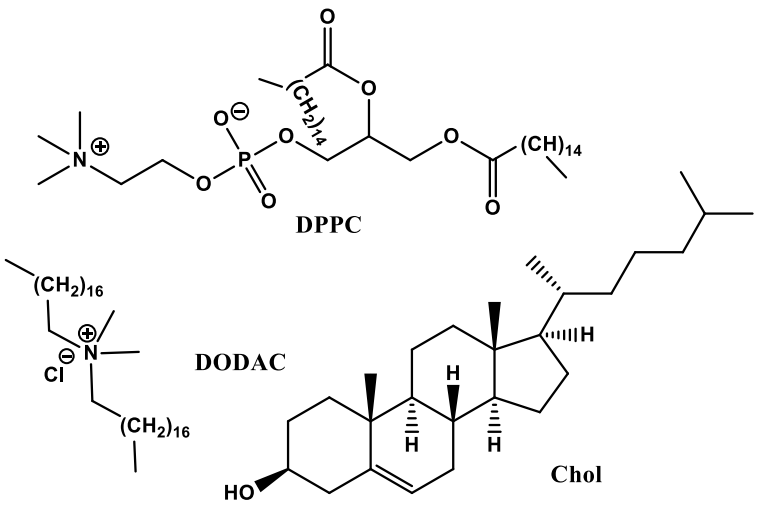

Figure 1. Structures of the components of the liposomal formulations: DODAC (dimethyldioctadecylammonium chloride), DPPC (dipalmitoylphosphatidylcholine), Chol (cholesterol).

The main component of liposomes is the zwitterionic lipid DPPC, which is fully saturated and, thus, is not affected by the radical species produced upon MB photoactivation. Cholesterol was added to the formulation to increase the fluidity of DPPC membrane and, thus, to improve the formation and stability of liposomes, as well as their possibility to interact with bacterial membranes. Finally, different amounts of a cationic lipid (DODAC) were employed to test the influence of electrostatic interactions of the carrier with the negatively charged bacterial membrane on the overall anti-bacterial efficacy of the compounds. Moreover, slightly different preparation protocols were employed for the different formulations, as described in the experimental section, in order to vary the size of the vesicles and, thus, to evaluate the effect of this parameter on bactericidal activity.

First, a physico-chemical characterization of the liposomal formulations was carried out by means of Dynamic Light Scattering (DLS) and Zeta Potential analysis. **Figure 2** compares the normalized autocorrelation functions (ACF) of the scattering intensity measured by DLS for all the formulations, while in **Table 2** the hydrodynamic diameter and polydispersity of liposomes,

obtained from the analysis of DLS curves through the cumulant fitting stopped at the second order, are reported for the different liposomal formulations, together with the Zeta Potential values.

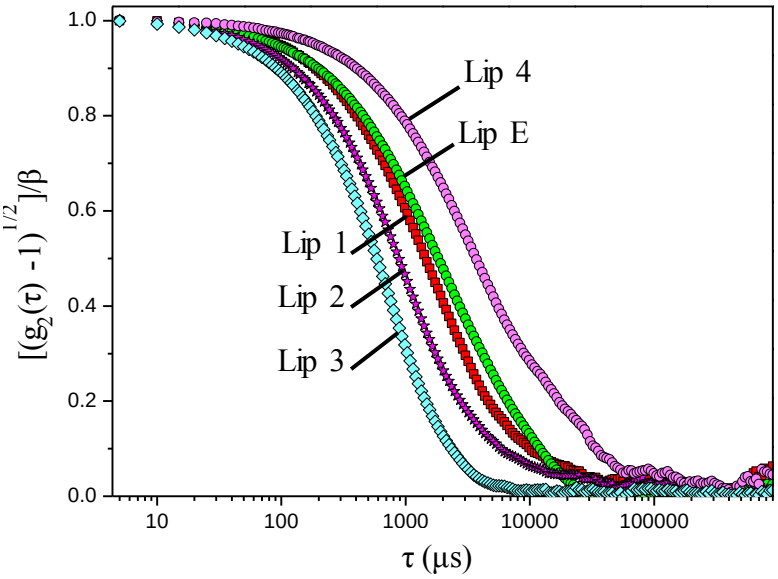

Figure 2. Normalized ACFs of the scattered intensity obtained by DLS for the five different liposomal formulations, one hour after preparation.

Table 2. Physicochemical features of the five different liposomal formulations, correlated with the evaporation time (minutes, Ev.) employed in the preparation protocol of each formulation; mean hydrodynamic diameter (Dh) and polydispersity index (PDI) obtained from the cumulant analysis stopped at the second order of the DLS curves and Zeta Potential values (ζ) are reported, together with the surface charge density of liposomes, calculated from Dh and ζ values, as reported in the **ESI**.

	Ev. (min)	**Dh (nm)**	**PDI**	**ζ (mV)**	**ρ (C/nm^2)**
Lip1	30	190 ± 20	0.336	45 ± 5	3.3×10^{-22}
Lip 2	90	160 ± 20	0.210	58 ± 5	5.0×10^{-22}
Lip 3	120	150 ± 10	0.072	63 ± 5	5.8×10^{-22}
Lip 4	10	240 ± 30	0.423	53 ± 8	3.1×10^{-22}
Lip E	30	210 ± 20	0.375	42 ± 5	2.8×10^{-22}

From the ACF profiles, the liposomal formulations appear to differ by both size and polydispersity. Clearly, the main factor affecting the final size and polydispersity of liposomes is the preparation method rather than the liposomal composition: as a matter of fact, similar sizes are obtained for the liposomes with intermediate DODAC amount (**Lip 2** and **Lip 3**), while larger and highly polydisperse vesicles are obtained both for the lowest (**Lip 1**) and highest (**Lip 4**) amount of DODAC. On the other hand, it is well established that a key step in reverse phase evaporation (REV) procedures is the mode of organic solvent evaporation, which directly influences the self-assembly kinetics of the lipid bilayer. Accordingly, we observed a clear trend to a decrease in size and polydispersity of the vesicles along with increasing the evaporation time, as reported in **Table 1**. Concerning the zeta potential values (see **Table 1**), the increase of the amount of cationic lipid component used in a formulation induces a parallel enhancement of the superficial charge of liposomes. Indeed, passing from a 16.6 % (**Lip 1**) to a 34.8 % (**Lip 3**) molar percentage of DODAC the zeta potential values rose from 45 up to 63 mV. Interestingly, a higher amount of DODAC (44.4 % in **Lip 4**) does not cause a corresponding increase in the superficial charge of liposome surfaces. This may be related to the presence of a maximum molar ratio of DODAC, beyond which the cationic lipid component can no longer be incorporated into the liposomal structure because of electrostatic repulsion, as previously reported for analogues SA-containing liposomes[32]. This feature was further confirmed for liposomes prepared with higher amounts of the cationic component (**ESI-Figure 1**). From the hydrodynamic radius of liposomes obtained from DLS and the corresponding zeta potential value, it is possible to calculate an estimate of the surface charge density of liposomes (**ESI**), obtaining an estimate of their surface charge density[29]. As expected, a clear difference comes out between **Lip 1** and **Lip 4**, which are of bigger size, more polydisperse and thus, characterized by a lower surface charge

density, with respect to **Lip 2** and **Lip 3**, that are characterized by a smaller size and lower PDI, leading to a higher surface charge density. Thus, it is clear that the preparation protocol adopted, and in particular the solvent evaporation time, has a major effect in the physicochemical features of the different liposomes, that might be of relevance in their efficiency as MB carriers for PDT applications. Finally, to investigate the stability of liposomes, DLS and zeta potential measurements were recorded on liposomal dispersions of the different formulations at different times after preparation: no significant changes either in the correlation functions or in the superficial charges were detected 2 months after their preparation (**ESI-Figure 2**). This relative high stability may be explained with the electrostatic repulsion between liposomes, due to the positive surface charge, which stabilizes the systems, avoiding aggregation.

Methylene blue encapsulation. It is well known that MB is partially associated in water in dimeric structures featuring a blue-shifted absorption band at 610 nm with respect to that of the monomer at 664 nm[33]. The dimerization process, whose equilibrium constant in water is 3.8 $x10^3$ M^{-1},[16] is strongly affected by concentration and depends on the ionic strength. Furthermore, it can be also influenced by the presence of charged interfaces (anionic polymers). Based on these considerations, spectrophotometric analysis of MB-containing liposome preparations before and after treatment with the nonionic surfactant Triton X100, which causes liposome disruption with formation of mixed micelles, can be considered as an evidence of the incorporation of MB into the nanostructures. **Figure 3** reports the UV-vis spectra of MB-containing liposomes dispersions, before and after addition of Triton X100, which induces the release of 100% MB from liposomal pool.

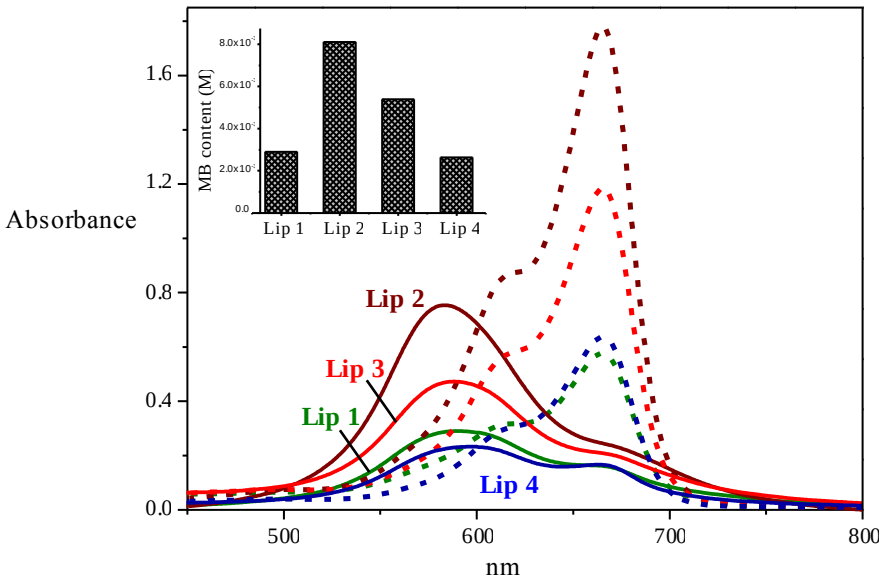

Figure 3. UV-vis spectra of MB-containing liposome preparations before (continuous lines) and after (dashed lines) treatment with Triton X100. Samples were diluted 1:300 in water; scattering of intact liposomes was corrected by subtraction of the absorbance of bare formulation; (inset) molar concentrations of MB encapsulated into liposomes, obtained from UV-vis analysis.

UV-vis spectra of intact MB-containing liposomes display a hypso-chromic effect with respect to non-encapsulated MB in water. Furthermore, a decrease of the molar absorbance at 664 nm and an increase of that at 610 nm with respect to free MB can be noticed, attributable to the enhancement of the dimer (DA) to monomer (MA) molar ratio. After treatment with Triton X100, MB spectra show an increase in the absorbance of the monomer form while the absorption band of the dimer disappears. This behavior suggests that MB is properly confined within liposomes and that the self-aggregation process is favored by its insertion into the liposomal nanostructure.

Loading of MB into liposomes is also confirmed by the analysis of its emission properties. In fact, the fluorescence emission registered for MB confined into nanostructures results in a less intense and blue shifted emission band with respect to that of free MB ($\Phi_F \sim 0.05$ in water)[34],

consistent with the significant decrease in fluorescence quantum yield due to the formation of self-assembled forms compared to that of the monomer species[35,36] (**ESI Figure 3**).

The amount of MB encapsulated into liposomes was evaluated through the construction of a calibration curve, obtained by measuring the absorbance values at 664 nm of a 1:300 dilution of Lip E (taken as negative control reference), containing Triton X100 (1%) and increasing amounts of MB (from 1 to 100 μM) (**ESI Figure 4**). By comparison of the absorbance values at 664 nm measured upon liposome disruption with the calibration curve described above, we determined the molar concentrations of MB originally confined into nanostructures, as shown in the inset of **Figure 3**. These vary from 2.63 x 10^{-3} M (**Lip 4**) to 8.10 x 10^{-3} M (**Lip 2**). Of note, the highest values were obtained for liposomes prepared under the longest times of solvent removal, which allow obtaining a more efficient reorganization of the lipid components and, thus limited leakage effects. Thus, from the displayed data, it is clear that the REV procedure is crucial to achieve high encapsulation of the active molecule inside liposomes and, moreover, it is confirmed that slow evaporation of the solvent is of paramount importance to guarantee low polydispersity of the liposomes and, accordingly, higher encapsulation efficiency.

Bactericidal efficacy of photo-activated MB-containg liposomes towards *E. coli*. To evaluate the ability of MB-containing liposomes as antibacterial agents for possible PDT application, we first tested their interaction ability towards *E. coli*, taken as a representative model of Gram-negative bacteria, in "dark conditions", i.e., in the absence of MB laser excitation.

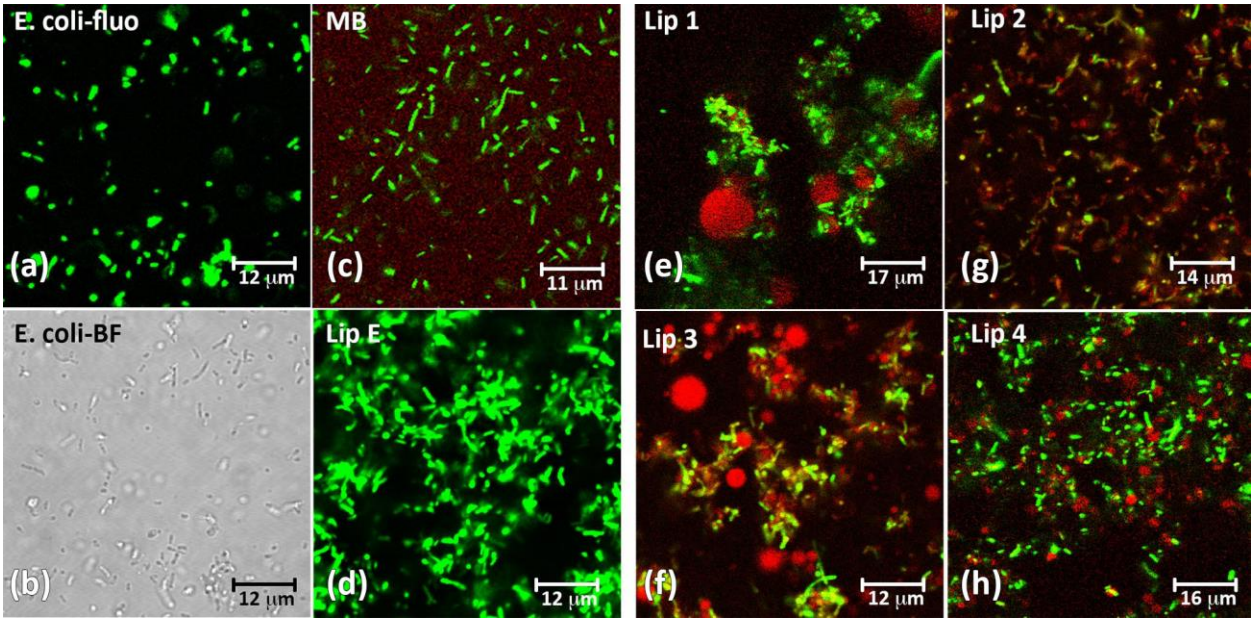

Figure 4. Representative CLSM images obtained for *E.coli* S17-1 strains pHC60 alone (a, b) and upon interaction with methylene blue (c) and with the different liposomal formulations (d-h). GFP-*E. coli* fluorescence ($\lambda_{excitation}$ =488 nm) is represented in green, while the bright field of the same sample is represented in greyscale, MB fluorescence ($\lambda_{excitation}$ =633 nm) is represented in red, GFP-MB fluorescence overlay is highlighted in yellow.

Figure 4a-b display representative CLSM images (in **Figure 4a** the GFP fluorescence, in **Figure 4b** the bright field image of the same field are displayed) of *E. coli* S17-1 strains constitutively expressing GFP laid on the bottom of a well. The GFP present inside the bacterial cytoplasm is characterized by a bright fluorescence emission in the 500-520 nm wavelength interval, which can be excited at $\lambda_{excitation}$ 488 nm. When the bacteria are incubated with a MB solution (see **Figure 4c**), no significant modifications in the bacteria are observed, moreover, MB fluorescence emission ($\lambda_{excitation}$ 630 nm, red) appears evenly distributed, without particular accumulation inside bacterial cytoplasm. When bacteria are challenged with the different liposomal formulations (**Figure 4d-h**), a clusterization of the bacteria is observed, attributable to a high tendency of liposomes to attach and adhere on the bacterial membrane, thus acting as bridges promoting the aggregation of bacteria themselves. Reasonably, the high density of

positive charges on the liposome surface gives rise to strong electrostatic interactions with the negative charges of the LPS coating of the outer bacterial membrane, resulting in the formation of liposomes-cells aggregates. Furthermore, the CLSM images displaying the *E. coli* samples challenged with MB-containing liposomes (**Figure 4e-h**) exhibit extensive areas where the fluorescence emission of GFP inside the bacterial cytoplasm (green) and that of MB (red) are colocalized (yellow), highlighting that MB is efficiently delivered inside *E. coli* cytoplasm by the different bacterial formulations. Spatially resolved emission spectra acquired for both GFP and MB in the same spots confirmed that colocalization of the fluorescent probes (GFP and MB) occurs for all the liposomal formulations tested (**ESI Figure 5**). Interestingly enough, bacteria challenged with **Lip 2** and **Lip 3** (**Figure 4g** and **Figure 4f**, respectively) seem to more extensively uptake MB, with respect to bacteria challenged with Lip 1 and Lip 4 (**Figure 4e** and **Figure 4h**, respectively), as highlighted by the different amount of yellow spots (i.e. GFP-MB colocalization regions) in the different samples. Even if this observation is not quantitative, it is worth noting that **Lip 2** and **Lip 3** are characterized by the longest solvent evaporation time in the preparation protocol, leading to smaller size of liposomes and lower polydispersity, and thus to a higher positive surface charge density with respect to **Lip 1** and **Lip 4** (see **Table 2**). This feature, together with the highest MB encapsulation efficiency values found for the **Lip 2** and **Lip 3** formulations, as discussed in the previous section, might be crucial in determining a better interaction of the liposomes with bacterial membrane, as well as a higher MB uptake inside bacterial cytoplasm.

Photo-activation experiments were carried out by irradiating for 60 seconds the photosensitizer agent with a diode laser with ($\lambda \geq 630$ nm, 200 mW), in order to compare the photo-induced

effect of liposomal formulations with the traditional treatment of periodontitis involving MB 0.02% w/v in water. Noteworthy, the absorption spectra recorded before and upon laser treatment on aqueous dispersions of liposomes did not show any significant enhancement of the absorbance at 664 nm, indicating that no MB was released in water as a consequence of irradiation. Thus, laser irradiation does not break the nanostructures (**Figure 6, ESI**).

The effect of photo-activated MB-containing liposomes on bacteria was evaluated by measuring bacterial titres both before and upon 60 seconds of laser irradiation of systems made up of *E. coli* S17-1 (1×10^9 cells/ml) treated with equal volumes of liposomal suspensions. As shown in **Figure 5**, which reports the viable counts obtained for the samples tested before and upon laser treatment, the different liposomal preparations featured different antibacterial activity. While **Lip E** and **Lip 4** seem to be only slightly effective upon photoactivation, comparable to an aqueous solution of MB 0.02 % (w/v) (t-test, $P > 0.05$), preparations **Lip 1**, **Lip 2** and **Lip 3** provoke a strong reduction in the bacterial titre. Furthermore, consistently with the CLSM data on the interaction of liposomes with bacteria discussed in the previous paragraph, **Lip 2** and **Lip 3** appear to be particularly efficient. In particular, **Lip 3** the most effective, causing an approx. 20-fold reduction of the titre as compared with MB alone (t-test, $P < 0.05$).

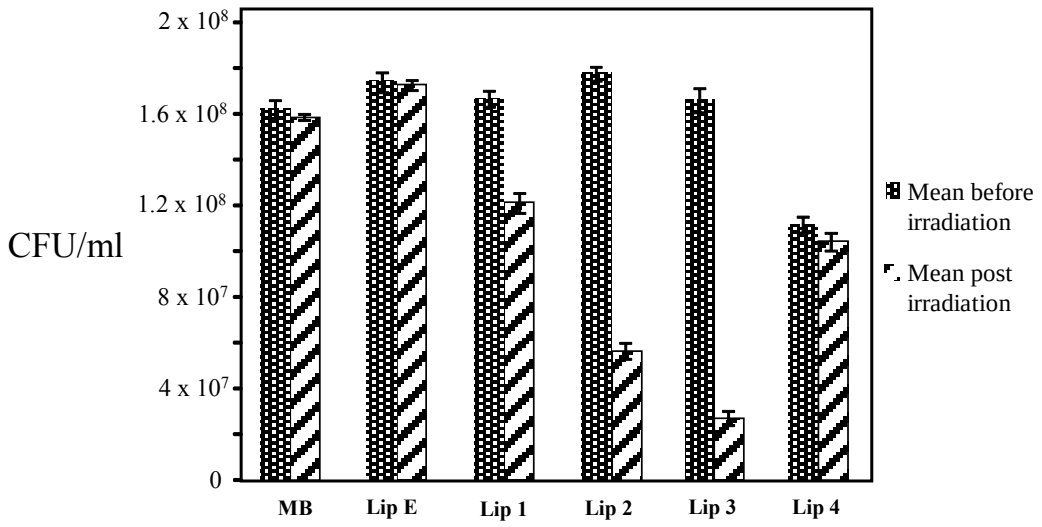

Figure 5 Bacterial titres of *E. coli* S-17-1 pHC60 before (blue) and after (red) laser treatment. Averages are related to three technical replicates.

To assess whether the observed reduction in cell viability was due to MB internalization mediated by liposomes, we replicated the same experiment by using *E. coli* pHC60 (expressing GFP) and collected CLSM images for liposome-cell systems with and without laser irradiation. **Figure 6** displays representative CLSM images of *E. coli* pHC60 incubated with bare MB (**Figure 6a-b**) and with MB-loaded **Lip 3** liposomes (**Figure 6c-d**), before (**Figure 6a, c**) and after (**Figure 6b, d**) MB laser excitation.

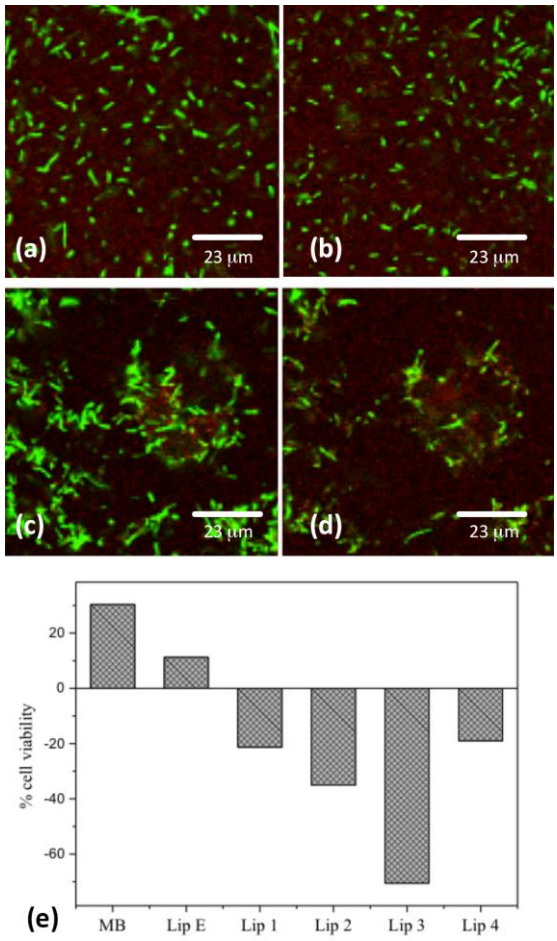

Figure 6. (a-d) CLSM measurements collected for systems made of E. coli S17-1 strains carrying pHC60 plasmid (constitutively expressing GFP) treated respectively with an aqueous solution of MB 0.02% w/v (a, b) and with Lip 3 (c, d) before (a, c) and after (b, d) 60 s of

irradiation with laser (λ = 630 nm, 200 mW). The images display GFP fluorescence emission ($\lambda_{excitation}$ 488 nm, green) overlaid with MB fluorescence emission ($\lambda_{excitation}$ 633 nm). (e) Bacterial titres of *E. coli* S17-1 pHC60 treated with the different MB-containing liposome formulations and MB 0.01%, after 10 minutes of laser treatment (λ = 630 nm, 60 s, 200 mW). Values determined through analysis of the CLSM images collected before, and upon treatment, by taking the GFP cellular fluorescence emission as a proxy of the cellular vitality.

Since the chosen strain of *E. coli* bacteria constitutively express GFP, the fluorescence emission of GFP can be is taken as a proof of cell viability. The comparison of GFP fluorescence spots (green) in the CLSM images acquired in the same regions before and after laser excitation for clearly show that GFP cellular fluorescence emission treated with liposome samples sharply decreases upon laser treatment, whereas using bare MB this is only slightly detected. A graphic counting of the GFP fluorescence emission, taken as an index of bacterial cell integrity/viability[37], provides a semiquantitative estimation of the bactericidal efficacies of the different liposomal formulations tested, which is summarized in the histogram in **Figure 6e**. The relative efficacy of the different system can be estimated as: **MB** < **Lip 4** < **Lip 1** < **Lip 2** < **Lip 3**. The bactericidal efficacy of the systems is thus consistent to what observed in dark conditions, with no laser excitation: **Lip 2** and **Lip 3** are the most efficient systems, and, in particular, **Lip 3**, which is characterized by the highest surface charge density, appears to be the most efficient.

In order to further explain this finding, we can consider that decrease in the cellular GFP fluorescence upon photoactivation of liposome formulations is particularly evident in the case of marked liposome-cell aggregates (see **Figure 6c-d**). This suggests that the formation of sticky aggregates liposome-cell is a key feature to enhance the bactericidal efficacy of liposomes, probably due to a higher concentration of MB and of ROS produced upon photoactivation, and this aggregation effect is clearly favored in the case of small liposomes with high surface charge density.

Finally, we investigated the ability of MB-containing liposomes to penetrate the biofilm of *E. coli* since, as already discussed, the activity of the PDT drugs against biofilm is one of the main open challenges for the development of PDT for antibacterial applications. The biofilm penetration abilities of liposome formulations was compared to that of MB 0.02% w/v. **Lip 3**, **Lip 2** and **Lip 1** were the most effective, while **Lip 4**, **Lip E**, and free MB did not significantly penetrate (see **ESI Figure 7**). This finding is in well agreement with the different bactericidal properties of the liposomes emerged from the photo-dynamic experiments and evidences that the biofilm penetration, as well the bactericidal efficacy, are markedly favored by high surface charge density of liposomes.

Evaluation of inflammatory activation of RAW 264.7 macrophages. An effective anti-microbial treatment should be able to reduce the bacterial load on one hand and to inactivate the bacterial pro-inflammatory by-products, such as LPS[38] Greenfield et al., 2005). In this context, we evaluated the ability of the different liposome preparations and free MB (0.02% w/v in water) to reduce the inflammatory activation of RAW 264.7 macrophages induced by the *Porphyromonas gingivalis* LPS adsorbed to titanium supports, after laser photo-excitation.

In **Figure 7** optical microscopy images are shown, highlighting the interaction pathway of liposomes with macrophage cells. Similarly to what observed on *E. coli* bacteria, liposomes tend to stick to the surface of RAW 264.7 macrophages and, in some cases, images of liposome internalization were observed suggesting the occurrence of phagocytosis. Thus, liposomes clearly closely interact with the RAW cells, eventually delivering the MB inside their cytoplasm.

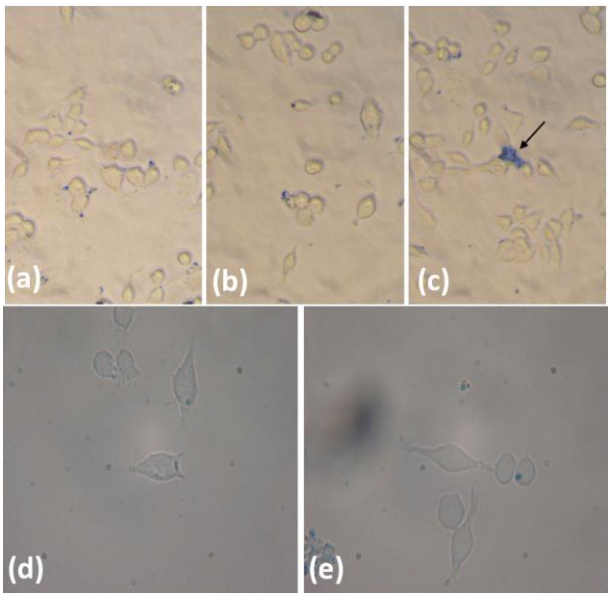

Figure 7 Images obtained by optical microscopy (OM) for samples containing RAW 264.7 (5 x 10^4 cells of in DMEM culture medium), treated with 20 µl of an aqueous dispersion of Lip 3 (a), Lip 2 (b) and Lip 4 (c). Liposome samples from the correspondent REV preparations were diluted in milliQ water to get a final [MB] of 6.25 x 10^{-4} M. (d-e) Images of the interaction of RAW 264.7 with Lip 3 (aqueous dispersion) obtained through optical microscopy (OM). Phenomena of phagocytosis are visible. (5 x 10^4 cells of RAW 264.7 in DMEM; liposome samples: 20 µl of a dilution 1/90 of the REV preparation).

Finally, RAW 264.7 cell activation upon laser application to macrophages incubated with the different formulations was evaluated. Cell activation was indirectly determined by measurement of nitrites, an index of NO generation by inflammation-challenged macrophages. To improve reliability of this test, the values of nitrites were normalized to cell viability, assayed by MTT. The main results are summarized in the histogram in **Figure 8**.

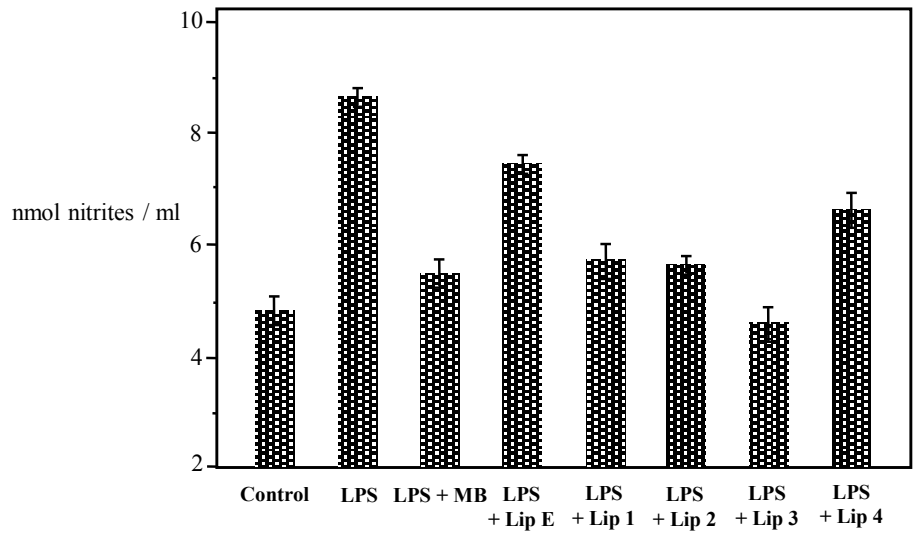

Figure 8. NO generation by RAW 264.7 macrophages, normalized respect on the cellular viability obtained from MTT assay, registered for the different liposomal formulations and for an aqueous solution of MB 0.02% w/v, upon irradiation for 1 minute with laser diode (630 nm, 200 mW). Means are related to three technical replicates. Cells seeded without any treatment were used as basal control, whereas cells stimulated for 24 h with LPS (50 mg/ml), represent the positive control.

Even if in this experiment the efficacy of the most active liposomes was found similar to that of free MB, probably due to the different structure and generally higher permeability of the eukaryotic cell membranes with respect to the bacterial ones, the various liposome formulations show different ability to inhibit the pro-inflammatory effects of LPS, the relative efficacy being: **Lip 3** > **Lip 2** > **Lip 1** > **Lip 4** > **Lip E**. Of note, the anti-LPS effect parallels the bactericidal efficacy and the penetrating ability into *E. coli* biofilm. Once again, the different efficacies seem to be correlated to the different physicochemical parameters of the different formulations, which are in turn connected with their preparation protocol: a slower solvent evaporation step in the REV procedure leads to smaller and less polydisperse liposomes, with higher surface charge density and higher MB encapsulation efficacy. Both these features (surface charge density and amount of MB inside the aqueous pool) can be connected to the efficacy in the interaction with

both bacterial and eukaryotic cells (as revealed by optical microscopy and CLSM images), in the amount of MB delivered inside the cells' cytoplasm and, finally, in the bactericidal activity.

CONCLUSIONS

In this study we have explored the chemical and anti-bacterial properties of MB, a well-known phenotiazinic dye employed in the photodynamic treatment of several inflammatory and infectious diseases, such as periodontitis, encapsulated into cationic liposomes with different characteristics. MB-loaded nanoparticles show a higher efficiency in terms of both bacterial cell toxicity and penetration into the bacterial biofilm, with respect to MB aqueous solutions. The enhanced antibacterial activity is accompanied by a strong detoxifying efficacy of the nanoparticles against the pro-inflammatory effect of Gram-LPS. Therefore, encapsulation of MB into cationic liposomes improve both its anti-bacterial and anti-inflammatory efficacy upon laser photoexcitation as compared with MB alone. These results could be well correlated with the protocol adopted for preparation of the different formulations and with the resulting physicochemical features of the liposomes. In fact, the preparation protocol was found to control the physicochemical features of MB-containing liposomes, both in terms surface charge density and MB encapsulation efficiency, factors that appeared crucial in the anti-bacterial and anti-inflammatory activity. These findings can contribute to fundamental knowledge, of great interest for further development of MB-liposomes for PDT application. MB nanoparticles hold great promise as photoactive antimicrobial drugs to specifically target Gram-bacteria and their harmful by-products, such as LPS. Although further investigations are needed to elucidate its possible efficacy against multiple bacterial species, the present MB-containing nanostructures are promising active principles as sensitizer agents in antibacterial PDT therapy.

EXPERIMENTAL PROCEDURES

Materials and Methods. All chemicals were of highest-reagent grade and used without further purification.

Preparation of Liposomes. MB-containing liposomes and bare liposomes without MB, were obtained using reverse phase evaporation (RPE) procedure reported by Szoka and Papahadjopoulos[39], with minor modifications. Briefly, a lipid mixture of dipalmitoylphosphatidylcholine (DPPC), cholesterol (Chol), and dimethyldioctadecylammonium chloride (DOTAC) was dissolved in chloroform by employing different lipid amounts as reported in **Figure 1b**. The solvent was removed under reduced pressure. The obtained lipids were dissolved under nitrogen in 3 ml of diethyl ether and added with either 1 ml of an aqueous solution of 0.1 M MB or milliQ water to prepare MB-containing of reference liposomes, respectively. The resulting two-phase systems were sonicated at 0-5 °C to obtain homogeneous opalescent dispersions. The organic solvent was then removed under reduced pressure at 25°C until the system collapsed, giving a viscous gel. During this phase, reverse micelles approach to each other and start to combine their lipid coatings, giving rise to the lipid bilayer and so to the reverse phase vesicles (REV) containing an internal aqueous phase. Keeping on evaporating solvent, we got an aqueous suspension of REV liposomes.

All the preparations were dialyzed in order to eliminate the MB non encapsulated into liposomes. With respect to the RPE procedure reported by Szoka and Papahadjopoulos, we employed greater sonication times of the two-phase systems, up to 30 minutes instead of 2-5 minutes.

This allowed to more efficiently break the interphase between the lipid and aqueous phase favoring the transfer of the photosensitizer from the aqueous to the lipid phase, thus maximizing MB encapsulation. Furthermore, following the formation of inverted micelles, a slow (up to two hours) removal of the organic solvent by rotary evaporation under reduced pressure was carried out in order to avoid the formation of foam or bubbles and achieve the formation of unilamellar liposomes with high MB encapsulation.

Electronic absorption and emission measurements. Absorption spectra of MB-containing liposomes were recorded on a Perkin-Elmer Lambda 6 spectrophotometer while fluorescence emission was recorded on a Perkin-Elmer LS55 spectrofluorimeter. Triton X100 (1% final concentration) was added to the solutions of liposomes to break the liposomal membrane down, allowing the release of MB into the solution. All the solutions used were not degassed and therefore were used with normal concentrations of O_2 present in the solvents, i.e. 10^{-3} M.

Dynamic Light Scattering. DLS measurements were performed on a Brookhaven Instrument 90 Plus (Brookhaven, Holtsville, NY), at $\theta = 90°$, T = 298 K. Each measurement was an average of five one-minute repetitions. All the samples were analyzed through the cumulant fitting stopped to the second order, allowing estimating the hydrodynamic diameter of particles and the polydispersity index. For simplicity, the same fitting procedure was adopted both for monodisperse liposomal formulations (for which the fitting is completely reliable) and for more polydisperse liposomal formulations (for which the cumulant analysis does not completely describe the whole profile of the curves), considering the main decay of the curves as the one relevant for the analysis. This approach was adopted in order to allow a better comparison of the different formulations.

Zeta Potential. Zeta potential measurements were taken using a zeta potential analyzer (Zeta Plus, Brookhaven Instruments Corporation, Holtsville, NY). Zeta potentials were obtained from the electrophoretic mobility u, according to the Helmholtz–Smoluchowski equation (equation 1):

$$\zeta = {}^{\eta}/_{\varepsilon} \times u \quad (1)$$

with η being the viscosity of the medium and ε the dielectric permittivity of the dispersing medium. The zeta potential values are reported as averages from 5 measurements on each sample.

Bacterial strains and culture conditions. An overnight culture of *E. coli* S17-1 strains carrying pHC60 plasmid constitutively expressing the Green Fluorescent Protein (GFP) grown in LB medium supplemented with 10 mg/L tetracycline at 37°C was pelleted by centrifugation at 6000 rpm for 10 minutes[40,41]. Cells were suspended in water for microscopic observation and treatment with MB-containing liposomes and MB.

Bacterial titres were determined by plating serial dilutions of bacterial cultures in LB plates supplemented with 10 mg/L tetracycline and incubated at 37°C overnight. Three replicas for each dilution were prepared. For the treatment of bacterial cells, an aliquot of 20 µl of *E. coli* S-17-1 cells resuspended in water was mixed with an equal volume of MB solution in water 0.02% w/v or liposomes suspension, each sample with a final molar concentration of MB of 62.5 µM, in a microtitre plate. After 10 minutes an aliquot of 10 µl of cells was used for determining pre-treatment viable titre. Then the remaining cell suspensions were treated with LED laser ($\lambda \geq 630$ nm, 200 mW) for 60 seconds. After 60 seconds an aliquot of 10 µl of cells was taken and used

for determining post-treatment viable titre. Fluorimetric measurement of cell integrity were also taken from CLSM images as reported in literature[37].

Static biofilm of *E. coli* S17-1 pHC60 cells was prepared by growing a pre-inoculum ($OD_{600\ nm}$ = 0.2) in 250 µl M9 broth (Sigma-Aldrich, Milan, Italy)ref) supplemented with 10 mg/L tetracycline in a 96-well microtiter for 24 h at 37°C, as described in literature[42]. To assess the ability of liposomes to interact (impregnate) bacterial biofilms, 200 µl of M9 broth were removed from wells and appropriate volumes of MB solution 0.02% or liposome suspensions were added at a final molar concentration of MB of 62.5 µM. After 10 minutes of incubation planctonic cells were removed by pipetting out the solution and washing three times each well with 200 µl of PBS buffer (NaCl 137 mM, KCl 2.7 mM, Na_2HPO_4 10 mM, KH_2PO_4 1.8 mM, pH=7.4). Adhesion of MB was then measured as absorbance of each well at λ = 600 nm.

Confocal Laser Scanning Microscopy. CLSM experiments were carried out with a confocal laser scanning microscope Leica TCS SP2 (Leica Microsystems GmbH, Wetzlar, Germany) equipped with a 63x water immersion objective. The 488 nm laser line was employed to detect the GFP-labeled *E. coli* (λ excitation 488 nm, λ emission 498-530 nm); the 633 nm laser line was employed to detect MB fluorescence (λ excitation 633 nm, λ emission 643-750 nm). For the measurements, 1 x 10^9 cells/ml of bacteria were put in a measurement chamber (Lab-Tek® Chambered # 1.0 Borosilicate Coverglass System, Nalge Nunc International, Rochester, NY USA) previously treated with a film of polylysine and then incubated with 20 µl of a reference solution of MB 0.02% w/v in water, or with appropriate volumes of each liposome suspension to achieve the same MB concentration as the bare MB solution, for 10 minutes, before the

acquisition of the images. For the photo-activation of bare and liposome-encapsulated MB, we irradiated the preparations with a low-energy diode laser ($\lambda \geq 630$ nm, 200 mW) for 60 seconds.

Evaluation of inflammatory activation of RAW 264.7 macrophages. The ability of photoexcited MB-containing liposomes or free MB to inactivate the Gram-negative endotoxin LPS was assessed by measuring its pro-inflammatory effects on macrophages in in vitro culture, as described in a previous work[43]. Mouse RAW 264.7 macrophages were obtained from American Type Culture Collection (ATCC, Manassas, VA). Cells were maintained in Dulbecco's Modified Eagle Medium (DMEM) supplemented with 10% fetal bovine serum (Gibco Invitrogen, Milan, Italy), 100U/ml penicillin–streptomycin, 1% l-glutamine 200 mM, (Sigma, St. Louis, MO) and 4.5 g/l glucose, and grown in 5% CO_2 atmosphere at 37 °C. Macrophages were seeded on titanium (Ti) discs, 5-mm diameter, 0.5–1 mm thick, cut from the terminal end of commercial dental implants (Bicon Dental implants, Boston, MA) and then cleaned and sterilized. Some of them were used with no further treatment, whereas others were coated with *E.coli* LPS (Sigma-Aldrich, Milan, Italy; 50 mg/ml).

The LPS-coated discs were immersed in 20 µl of an aqueous solution of MB 0.02% w/v or in proper volumes of aqueous dispersion of MB-containing liposomes to achieve the same final molar concentration of MB in the reference, and then irradiated for 30 seconds on each side (1 minute in total), with a diode laser ($\lambda \geq 630$ nm, 200 mW), at a distance of 2 mm from the solution surface and with an angle of 90°. The discs were individually placed into the wells of a 96-well plate, in contact with the seeded macrophages (2×10^5 cells). Cultures were maintained for 24 h in 250 ml of DMEM, supplemented with 20% fetal bovine serum. Cells seeded into 96-

well plate without any treatment were used as basal controls, whereas cells stimulated for 24 h with LPS (50 mg/ml), directly added to the culture medium, were used as positive controls.

The generation of nitrites, stable end-metabolites of nitric oxide (NO), a typical inflammatory products of activated macrophages[44,45], was revealed by the Griess reaction and quantitated spectrophotometrically at λ 546 nm absorbance, in comparison with a standard curve of $NaNO_2$. The reported values are the mean of triplicate experiments and are expressed as nmol/ml. These values were then normalized to cell viability, evaluated by the MTS assay.

MTS cell viability assay. RAW 264.7 cell viability upon the different treatments was assayed by the MTS CellTiter 96 Aqueous One Solution Assay (Promega, Milan, Italy). Aliquots of RAW 264.7 (2 x 10^5 cells) were placed in a 96-well cell culture plate in 250 ml phenol red-free DMEM/well. Some wells contained LPS-coated Ti discs were pre-treated with photo-activated MB 0.02% w/v or MB-containing liposomes. Cells placed into the wells without any treatment, seeded on uncoated Ti discs or stimulated for 24 h with LPS (50 mg/ml) directly added to the culture medium, were used as negative and positive controls, respectively. After 24 h, 20 ml of MTS solution were added to each well and the plates were incubated at 37°C for 3 h. The absorbance of the product formazan, which is considered to be directly proportional to the number of living cells in the culture, was measured at 490 nm and 650 nm wavelength using a microplate spectrophotometer (Molecular Devices, Sunnyvale, CA).

ACKNOWLEDGMENTS

Bibliography

(1) Petelin, M., Perkič, K., Seme, K., and Gašpirc, B. (2015) Effect of repeated adjunctive

antimicrobial photodynamic therapy on subgingival periodontal pathogens in the treatment of chronic periodontitis. *Lasers Med. Sci. 30*, 1647–1656.
(2) Usuda, J., Tsutsui, H., Honda, H., Ichinose, S., Ishizumi, T., Hirata, T., Inoue, T., Ohtani, K., Maehara, S., Imai, K., Tsunoda, Y., Kubota, M., Ikeda, N., Furukawa, K., Okunaka, T., and Kato, H. (2007) Photodynamic therapy for lung cancers based on novel photodynamic diagnosis using talaporfin sodium (NPe6) and autofluorescence bronchoscopy. *Lung Cancer 58*, 317–323.
(3) Plaetzer, K., Berneburg, M., Kiesslich, T., and Maisch, T. (2013) New applications of photodynamic therapy in biomedicine and biotechnology. *Biomed Res. Int.*
(4) Debele, T. A., Peng, S., and Tsai, H. C. (2015) Drug carrier for photodynamic cancer therapy. *Int. J. Mol. Sci.*
(5) Kamkaew, A., Lim, S. H., Lee, H. B., Kiew, L. V., Chung, L. Y., and Burgess, K. (2013) BODIPY dyes in photodynamic therapy. *Chem. Soc. Rev. 42*, 77–88.
(6) Diniz, I. M. A., Horta, I. D., Azevedo, C. S., Elmadjian, T. R., Matos, A. B., Simionato, M. R. L., and Marques, M. M. (2015) Antimicrobial photodynamic therapy: A promise candidate for caries lesions treatment. *Photodiagnosis Photodyn. Ther. 12*, 511–518.
(7) Biel, M. A. (1998) Photodynamic therapy and the treatment of head and neck neoplasia. *Laryngoscope 108*, 1259–1268.
(8) Bown, S. G., Rogowska, A. Z., Whitelaw, D. E., Lees, W. R., Lovat, L. B., Ripley, P., Jones, L., Wyld, P., Gillams, A., and Hatfield, A. W. R. (2002) Photodynamic therapy for cancer of the pancreas. *Gut 50*, 549–57.
(9) Dolmans, D. E. J. G. J., Fukumura, D., and Jain, R. K. (2003) Photodynamic therapy for cancer. *Nat. Rev. Cancer 3*, 380–387.
(10) Kawczyk-Krupka, A., Bugaj, A. M., Latos, W., Zaremba, K., Wawrzyniec, K., and Sieroń, A. (2015) Photodynamic therapy in colorectal cancer treatment: The state of the art in clinical trials. *Photodiagnosis Photodyn. Ther.*
(11) Dougherty, T. J., Gomer, C. J., Henderson, B. W., Jori, G., Kessel, D., Korbelik, M., Moan, J., and Peng, Q. (1998) Photodynamic therapy. *J. Natl. Cancer Inst. 90*, 889–905.
(12) Ericson, M. B., Wennberg, A.-M., and Larkö, O. (2008) Review of photodynamic therapy in actinic keratosis and basal cell carcinoma. *Ther. Clin. Risk Manag. 4*, 1–9.
(13) Song, B. H., Lee, D. H., Kim, B. C., Ku, S. H., Park, E. J., Kwon, I. H., Kim, K. H., and Kim, K. J. (2014) Photodynamic therapy using chlorophyll-a in the treatment of acne vulgaris: A randomized, single-blind, split-face study. *J. Am. Acad. Dermatol. 71*, 764–771.
(14) Allison, R. R., and Moghissi, K. (2013) Photodynamic therapy (PDT): PDT mechanisms. *Clin. Endosc. 46*, 24–29.
(15) Huang, L., Xuan, Y., Koide, Y., Zhiyentayev, T., Tanaka, M., and Hamblin, M. R. (2012) Type i and Type II mechanisms of antimicrobial photodynamic therapy: An in vitro study on gram-negative and gram-positive bacteria. *Lasers Surg. Med. 44*, 490–499.
(16) Tardivo, J. P., Del Giglio, A., De Oliveira, C. S., Gabrielli, D. S., Junqueira, H. C., Tada, D. B., Severino, D., De F??tima Turchiello, R., and Baptista, M. S. (2005) Methylene blue in photodynamic therapy: From basic mechanisms to clinical applications. *Photodiagnosis Photodyn. Ther.*
(17) Castano, A. P., Demidova, T. N., and Hamblin, M. R. (2005) Mechanisms in photodynamic therapy: Part three - Photosensitizer pharmacokinetics, biodistribution, tumor localization and modes of tumor destruction. *Photodiagnosis Photodyn. Ther.*
(18) Triesscheijn, M., Baas, P., Schellens, J. H., and Stewart, F. A. (2006) Photodynamic therapy in oncology. *Oncologist 11*, 1034–1044.

(19) Maisch, T., Szeimies, R.-M., Lehn, N., and Abels, C. (2005) [Antibacterial photodynamic therapy. A new treatment for superficial bacterial infections?]. *Hautarzt. 56*, 1048–55.
(20) Kharkwal, G. B., Sharma, S. K., Huang, Y., and Dai, T. (2012) Photodynamic Therapy for Infections: Clinical Applications. *Lasers Surg Med. 43*, 755–767.
(21) Mielczarek-Badora, E., and Szulc, M. (2013) Photodynamic therapy and its role in periodontitis treatment. *Postepy Hig. Med. Dosw. 67*, 1058–1065.
(22) Sperandio, F. F., Huang, Y.-Y., and Hamblin, M. R. (2013) Antimicrobial Photodynamic Therapy to Kill Gram-negative Bacteria. *Recent Pat Antiinfect Drug Discov 8*, 1–23.
(23) Malik, Z., Hanania, J., and Nitzan, Y. (1990) Bactericidal effects of photoactivated porphyrins--an alternative approach to antimicrobial drugs. *J. Photochem. Photobiol. B.*
(24) Hamblin, M. R., and Hasan, T. (2004) Photodynamic therapy: a new antimicrobial approach to infectious disease? *Photochem. Photobiol. Sci. 3*, 436–450.
(25) Garcez, A. S., Núñez, S. C., Azambuja, N., Fregnani, E. R., Rodriguez, H. M. H., Hamblin, M. R., Suzuki, H., and Ribeiro, M. S. (2013) Effects of photodynamic therapy on Gram-positive and Gram-negative bacterial biofilms by bioluminescence imaging and scanning electron microscopic analysis. *Photomed. Laser Surg. 31*, 519–25.
(26) Høiby, N., Ciofu, O., Johansen, H. K., Song, Z., Moser, C., Jensen, P. Ø., Molin, S., Givskov, M., Tolker-Nielsen, T., and Bjarnsholt, T. (2011) The clinical impact of bacterial biofilms. *Int. J. Oral Sci. 3*, 55–65.
(27) H??iby, N., Bjarnsholt, T., Givskov, M., Molin, S., and Ciofu, O. (2010) Antibiotic resistance of bacterial biofilms. *Int. J. Antimicrob. Agents*.
(28) Bettoschi, A., Bencini, A., Berti, D., Caltagirone, C., Conti, L., Demurtas, D., Giorgi, C., Isaia, F., Lippolis, V., Mamusa, M., and Murgia, S. (2015) Highly stable ionic liquid-in-water emulsions as a new class of fluorescent sensors for metal ions: the case study of Fe\n 3+\n sensing. *RSC Adv. 5*, 37385–37391.
(29) Montis, C., Milani, S., Berti, D., and Baglioni, P. (2012) Complexes of nucleolipid liposomes with single-stranded and double-stranded nucleic acids. *J. Colloid Interface Sci. 373*, 57–68.
(30) Montis, C., Baglioni, P., and Berti, D. (2014) Monitoring the interaction of nucleolipoplexes with model membranes. *Soft Matter 10*, 39–43.
(31) Montis, C., Sostegni, S., Milani, S., Baglioni, P., and Berti, D. (2014) Biocompatible Cationic Lipids for the Formulation of Liposomal DNA Vectors. *Soft Matter 10*, 4287–97.
(32) Kim, H. J., Michael Gias, E. L., and Jones, M. N. (1999) The adsorption of cationic liposomes to Staphylococcus aureus biofilms, in *Colloids and Surfaces A: Physicochemical and Engineering Aspects*, pp 561–570.
(33) Mills, A., and Wang, J. (1999) Photobleaching of methylene blue sensitised by TiO2: an ambiguous system? *J. Photochem. Photobiol. A Chem. 127*, 123–134.
(34) Dean, J. C., Oblinsky, D. G., Rafiq, S., and Scholes, G. D. (2016) Methylene Blue Exciton States Steer Nonradiative Relaxation: Ultrafast Spectroscopy of Methylene Blue Dimer. *J. Phys. Chem. B 120*, 440–454.
(35) Morgounova, E., Shao, Q., Hackel, B. J., Thomas, D. D., and Ashkenazi, S. (2013) Photoacoustic lifetime contrast between methylene blue monomers and self-quenched dimers as a model for dual-labeled activatable probes. *J. Biomed. Opt. 18*, 56004.
(36) Severino, D., and Junqueira, H. C. (2003) Influence of Negatively Charged Interfaces on the Ground and Excited State Properties of Methylene Blue¶. *Photochem. ….*
(37) Choi, H., Yang, Z., and Weisshaar, J. C. (2015) Single-cell, real-time detection of oxidative

stress induced in Escherichia coli by the antimicrobial peptide CM15. *Proc. Natl. Acad. Sci.* 201417703.
(38) Nair, S. P., Meghji, S., Wilson, M., Reddi, K., White, P., and Henderson, B. (1996) Bacterially induced bone destruction: Mechanisms and misconceptions. *Infect. Immun.*
(39) Szoka, F., and Papahadjopoulos, D. (1978) Procedure for preparation of liposomes with large internal aqueous space and high capture by reverse-phase evaporation. *Proc. Natl. Acad. Sci. U. S. A. 75*, 4194–8.
(40) Cheng, H. P., and Walker, G. C. (1998) Succinoglycan is required for initiation and elongation of infection threads during nodulation of alfalfa by Rhizobium meliloti. *J. Bacteriol. 180*, 5183–5191.
(41) BERTANI, G. (1951) Studies on lysogenesis. I. The mode of phage liberation by lysogenic Escherichia coli. *J. Bacteriol. 62*, 293–300.
(42) O'Toole, G. a., Pratt, L. a., Watnick, P. I., Newman, D. K., Weaver, V. B., and Kolter, R. (1999) [6] Genetic approaches to study of biofilms. *Methods Enzymol. 310*, 91–109.
(43) Giannelli, M., Bani, D., Tani, A., Pini, A., Margheri, M., Zecchi-Orlandini, S., Tonelli, P., and Formigli, L. (2009) In vitro evaluation of the effects of low-intensity Nd:YAG laser irradiation on the inflammatory reaction elicited by bacterial lipopolysaccharide adherent to titanium dental implants. *J. Periodontol. 80*, 977–84.
(44) Moncada, S. P. and H. (1991) Nitric Oxide: Physiology, pathophysiology and pharmacology. *Pharmacol. Rev. 43*, 109–142.
(45) Masini, E., Nistri, S., Vannacci, A., Bani Sacchi, T., Novelli, A., and Bani, D. (2004) Relaxin inhibits the activation of human neutrophils: involvement of the nitric oxide pathway. *Endocrinology 145*, 1106–1112.